Nb$_2$O$_5$/SBA-15 catalyzed propanoic acid esterification

Ângela Silva [a,b], Karen Wilson [c], Adam F. Lee [c], Vannia Cristina dos Santos [c],
Ana Carolina Cons Bacilla [a], Karen Mary Mantovani [a], Shirley Nakagaki [a,*]

[a] *Laboratório de Bioinorgânica e Catálise, Universidade Federal do Paraná (UFPR), Departamento de Química, CP 19081, CEP 81531-990 Curitiba, Paraná, Brazil*
[b] *Instituto Federal de Santa Catarina (IFSC), Campus Chapecó, Rua Nereu Ramos, 3450 D, CEP 89813-000 Chapecó, Santa Catarina, Brazil*
[c] *European Bioenergy Research Institute, Aston University, Birmingham B4 7ET, UK*

ARTICLE INFO

ABSTRACT

A family of niobia (Nb$_2$O$_5$) functionalized SBA-15 solid catalysts have been prepared via wet impregnation with NbCl$_5$ (2–32 wt% Nb) and subsequent thermal processing, for application in the acid catalyzed esterification of propanoic acid with methanol. Bulk and surface physicochemical characterization revealed that highly dispersed niobia species present at low loadings when calcined at 500 °C exhibit strong Brönsted acid character and associated activity for esterification. Increased calcination temperatures are found to result in a decrease in Brönsted:Lewis acid ratio associated with recrystallization of the niobia phase leading to a loss of catalyst activity. Esterification activity is found to be directly proportional to Brönsted:Lewis acid ratio, with the 2 wt% Nb/SBA-15 catalyst pre-calcined at 500 °C found to exhibit highest activity and excellent reusability without deactivation.

© 2017 Elsevier B.V. All rights reserved.

1. Introduction

Humanity faces unprecedented environmental, social, and economic challenges in the 21st century due to population growth, with an associated *per capita* increase in the consumption of natural resources and a continued reliance on fossil fuels for both energy and chemicals production [1]. The search for alternative renewable energy sources has attracted attention in large part due to anthropogenic climate change, with biomass emerging as a front-runner for provision of liquid transportation fuels [1–5]. Biodiesel is the best established and commercially most widely available biomass derived fuel that has been introduced in the energy matrix of various countries (notably Brazil), with the goal of reducing air pollution and increasing both energy security and economic benefits [6,7]. Biodiesel is a good substitute for conventional diesel and can be obtained from vegetable oils, animal fats, fatty acids or waste fatty materials from residual cooking oils [7–10]. Waste raw materials are advantageous for biodiesel production since they do not compete with food applications or require land use change and offer lower cost production [11]. Biodiesel is conventionally synthesized through the transesterification of triacylglyceride components and esterification of fatty acid components, of vegetable oils and fats with light alcohols; excess alcohol is usually employed in order to drive the equilibrium towards the desired fatty acid alkyl ester (biodiesel) product [6,7]. Although transesterification is more rapid when catalyzed by base than by acid catalysts, the presence of free fatty acid (FFA) impurities in most oil/fat feedstocks hinders the use of the former due to soap formation and attendant energy intensive biodiesel separation [7]. Fatty acid esterification may be catalyzed by mineral or organic acids, such as sulfuric or *p*-toluenesulfonic acid [7,8], however the corrosive and toxic nature of these liquid acids and the requirement for their neutralization and separation increases process costs and lowers the green credentials of biodiesel [7,8].

Solid acid catalysts offer economic and process benefits, especially so for low cost feedstocks with high FFA content, enabling one-pot esterification and transesterification of bio-oils [12]. A wide range of solid acids [13], including heteropolyacids [14,15], sulfonated metal oxides [16,17] and carbons [18], and zeolites [19] have been applied to biodiesel production, however new materials with improved solvothermal stability and recyclability are still sought. Aranda et al. reported on the application of bulk niobia for biodiesel production from the esterification of palm oil which is high in FFAs, including palmitic (46.4%), oleic (41.2%) and linoleic

(11.1%) acids [20]; a net FFA conversion of around 80% was achieved with methanol at 130 °C. Niobic acid and niobium phosphate have also been applied for the esterification of C_{12} and C_{18} FFAs with methanol, ethanol and butanol. Amorphous niobium phosphate exhibited strong Brönsted acidity comparable to niobic acid, proving efficacious for lauric acid esterification with butanol [21].

Mesoporous materials are attractive in heterogeneous catalysis due to their high surface areas, tunable pore architectures and associated improved mass-transport, and ability to generate highly dispersed and active sites [22]. For example, SBA-15 mesoporous silica was recently used to stabilize dispersed conformal zirconia and sulfated zirconia monolayers for the synthesis of either ethyl levulinate or 5-hydroxymethylfurfural from glucose [23,24], and alkali-free hydrotalcite nanocrystals for biodiesel production from triacylglycerides [25]. Nb/SBA-15 has been explored by Calvino-Casilda et al. who studied the impact of Zr, Nb and Mo modified SBA-15 in Knoevenagel condensation, along with a series of bifunctional materials based on modified SBA-15 co-functionalized by aminopropyl groups. Nb/SBA-15 co-functionalised with propylamine groups showed the highest activity, which was attributed to a strong interaction between Nb cations and the silica support generating Lewis acidity [26,27]. Nb/SBA-15 has also been prepared in the presence of grafted propylsulfonic acid groups for use in glycerol esterification with acetic acid, in which Nb appeared to improve the stability of sulfonic acid functions, resulting in 66% glycerol conversion and 35% selectivity to triacetylglycerol [28,29]. Sumiya et al. also prepared Nb/SBA-15 comprising hydrated niobia (niobic acid) through treatment of a colloidal niobium oxide solution in the presence of the silica support. The resulting material exhibited high thermal stability and was more active for sucrose hydrolysis than bulk niobic acid [30].

Surprisingly despite the interest in niobia based catalysts and importance of esterification reactions for both chemical and biofuels production, a systematic study of the structure activity relationships in Nb/SBA-15 materials has not yet been reported for esterification reactions. Here we explore the potential of SBA-15 supported niobium for the esterification of propanoic acid as a model reaction to assess its potential for biodiesel production, and associated structure-function relations, notably the significance of Brönsted:Lewis character in dictating activity.

2. Experimental

2.1. Preparation of SBA-15

Mesoporous SBA-15 was synthesized following the method reported by Zhao and co-workers [31,32]. In a typical procedure, 16 g of Pluronic P123 (Aldrich, 96%) were dissolved in 500 mL of aqueous hydrochloric acid (1.9 mol/L) in a round bottom flask at room temperature. After complete dissolution, the mixture was warmed up to 35 °C and 28 g of TEOS (Aldrich) were added dropwise in a single step. The solution was then vigorously stirred for 24 h at 35 °C and hydrothermally aged at 80 °C for another 48 h. The solid product was then recovered by filtration and air-dried. Finally, surfactant was removed from inside the porous structure by calcination in static air at 550 °C for 5 h to give the product as a white powder.

2.2. Preparation of xNb/SBA-15(y) materials

Mesoporous silica supported niobium species were prepared by impregnation of SBA-15 with $NbCl_5$ in an isopropanol solvent, following the procedure of Chae et al. [33]. 3 g of SBA-15 was added to 30 mL of deionized water, 20 mL of isopropanol (Fisher Scientific) and an appropriate mass of niobium pentachloride ($NbCl_5$) (Aldrich,

99%) to obtain solids with niobium loadings spanning 2–32 wt% (theoretical loadings). The reaction mixture was stirred at room temperature for 24 h, and the liquid phase subsequently evaporated at 80 °C. The resulting solid was calcined subsequently at 500, 600 or 800 °C for 5 h (ramp rate 1 °C min^{-1}). The final materials are designated xNb/SBA-15(y), where x is the theoretical Nb loading and y is the solid calcination temperatures in Celsius degree (°C). Actual Nb loadings were obtained by XPS.

2.3. Materials characterisation

Nitrogen adsorption isotherms were obtained on a Quantachrome NOVA 4000e gas sorption analyzer using NovaWin software. Samples were degassed at 120 °C in vacuo overnight. Analyses were carried out under liquid nitrogen (−196 °C) and adsorption/desorption isotherms for N_2 were obtained over the relative pressure range 0.01–0.99. Specific surface areas were calculated using the multi-point Brunauer–Emmet–Teller (BET) method over the relative pressure range 0.01–0.3. Pore sizes were calculated from analysis of the desorption branch using the Barrett–Joyner–Halenda model (BJH) or Horvath-Kawazoe (HK) model with relative pressures >0.35 and <0.02 respectively. Powder XRD patterns were recorded on a PANalytical X'pertPro diffractometer fitted with an X'celerator detector and Cu-K a source for $2\theta = 0$ to 5° (small angle) and $2\theta = 10$ to 80° (wide angle) with a step size of 0.02°. The Scherrer equation was used to calculate Nb crystallite sizes. XPS analysis was performed on a Kratos Axis HSi X-ray photoelectron spectrometer fitted with a charge neutralizer and magnetic focusing lens employing Al Ka monochromated radiation (1486.7 eV). Spectral fitting was performed using CasaXPS version 2.3.15. Binding energies were corrected to the C 1s peak at 284.5 eV. HRTEM analysis was carried out on a JEOL/JEM instrument operating at 100–120 kV (dispersed in ethanol and dropped onto a grid). Dark-field images obtained in STEM mode. Diffuse reflectance UV–vis analyses (DRUV) were made using a Thermo Scientific™ Evolution 201/220 spectrophotometer, for wavelengths between 190 and 800 nm. Acid properties were determined by DRIFTS on a Nicolet IS50FT-IR Thermo Scientific™ spectrometer, through pyridine adsorption at room temperature. Approximately 1 mL of pyridine (Aldrich, 99.8%) was adsorbed on 200 mg of sample, which was dried overnight in a vacuum oven prior to analysis in order to remove physisorbed pyridine.

2.4. Catalytic activity

Esterification was performed in a Radley's Carousel reaction station under reflux using a 50 mL double neck round-bottomed flask. Reactions were conducted using 10 mmol of propanoic acid in 12.5 mL of methanol (molar ratio MeOH:acid = 30), at 60 °C, using 50 mg of catalyst and 0.12 mL of dihexylether as an internal standard. Reactions were periodically sampled for kinetic analysis using a Varian450 GC equipped with Phenomenex ZB-5HT Inferno wide bore capillary column (15 m × 0.32 mm × 0.10 μm), with analysis performed in triplicate. Recycle experiments were also conducted with the most active 2Nb/SBA-15(500) sample under solvothermal conditions, in which 50 mg of catalyst was placed inside a 15 mL Teflon liner with 10 mmol of propionic acid and 6.25 mL of methanol (molar ratio MeOH/acid = 15). The liner was then placed inside a stainless steel autoclave and put in a silicone oil bath and heated to 120 °C for 4 h under magnetic stirring at 800 rpm. After cooling to room temperature, excess alcohol in the supernatant solution was removed by vacuum evaporation, and fatty acid conversion to the corresponding propyl ester assayed by titration of the remaining acidity with NaOH (0.01 mol/L). The spent catalyst

was filtered, thoroughly washed with ethanol, and dried at 120 °C prior to re-use.

3. Results and discussion
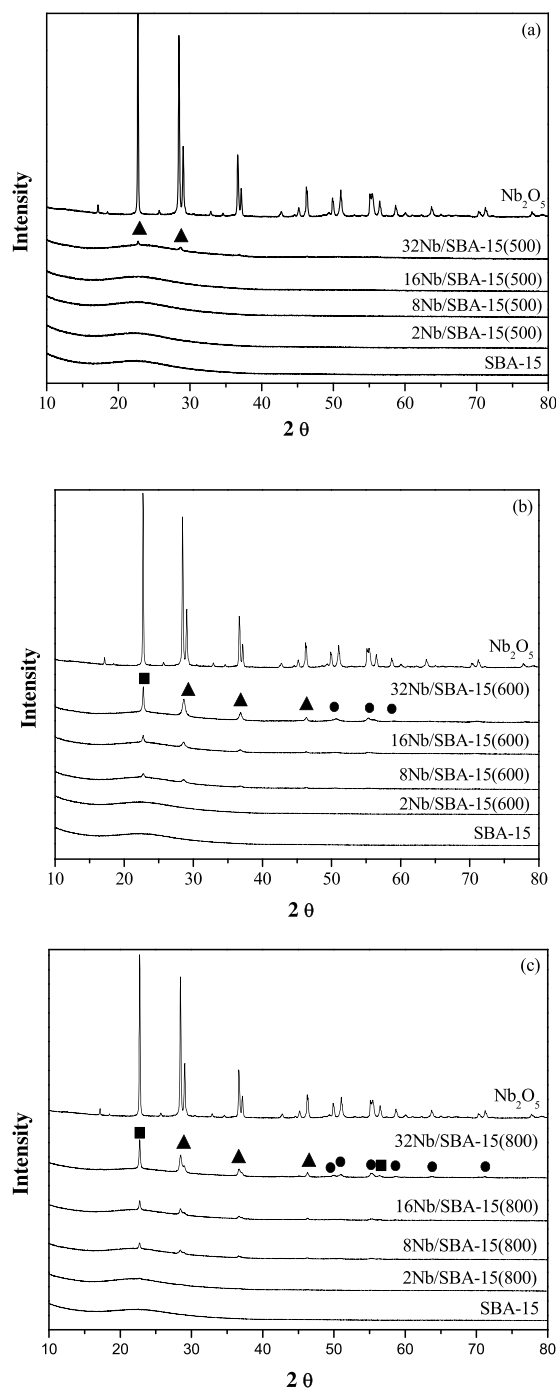
3.1. Solid catalyst characterization

Preservation of the parent SBA-15 mesopore structure following impregnation and high temperature thermal processing was first confirmed through N_2 porosimetry and low angle XRD (Figs. S1 and S2). All niobia (Nb_2O_5) functionalized SBA-15 materials exhibited type IV isotherms, analogous to that of the parent SBA-15, with BET surface areas decreasing with increasing Nb loading and calcination temperature, falling from ~750 $m^2 g^{-1}$ for the parent SBA-15 to around 500 $m^2 g^{-1}$ for the highest 32Nb/SBA-15(800) material after 800 °C calcination (Table S1). Low angle XRD (Fig. S3) revealed patterns characteristic of hexagonal close-packed *p6mm* mesoporous SBA-15 silica with three well-defined (100), (110), and (200) reflections in all materials [31–33].

Wide angle XRD failed to exhibit any Nb phase for loadings <2 wt% irrespective of calcination temperatures, indicating highly dispersed niobium, likely as an amorphous oxide phase [34] or atomically-dispersed within the SBA-15 framework (Fig. 1). Higher loadings and calcination temperatures resulted in the progressive evolution of bulk niobium phases, consistent with the formation of pseudohexagonal (TT) and orthorhombic (T) niobia below 500 °C, and additional reflections due to monoclinic (α) niobia above 600 °C, in accordance with literature expectations for unsupported niobia [34–41]. Nowak and Ziolek reported that the structural complexity and polymorphism of niobia is a strong function of the synthesis method, notably nature of the Nb precursor, processing time and temperature [35].

Crystallite size increased with Nb concentration and calcination temperature [42–46]. Particle sizes of crystalline niobia phases were estimated for the 32Nb/SBA-15 sample from line broadening of the 22.5° reflection in Fig. 2, by application of the Scherrer equation, revealing a small increase from 35.5 to 41.2 nm after calcination at 500 °C and 800 °C respectively. These are similar to literature values for pure Nb_2O_5/SiO_2 [34] but smaller than calculated for commercial niobium oxide (58.5 nm) which comprised a mixture of orthorhombic (T) and monoclinic (α) niobia. Silica thus appears to play an important role in stabilizing dispersed niobium against particle sintering, even after aggressive calcination treatments, which was attributed previously to a strong niobia-silica interaction and Nb—O—Si bond formation [47], although niobium mobility clearly increased at higher temperature.

DRUV analyses showed that niobium incorporation resulted in the emergence of a strong and broad absorbance between 200 and 400 nm, consistent with that observed for pure niobia (Fig. S4). This has been previously assigned to the presence of at least two different Nb species [34,48,49], with features around 220 nm arising from tetrahedral niobium species coordinated to MCM-41 and SBA-15 silica support [28,29,50–55], and those around 330 nm due to octahedral Nb present within extra framework Nb_2O_5. The intensity of the higher wavelength band increased with Nb loading, in accordance with the appearance of crystalline Nb_2O_5 observed by XRD.

The Nb 3d XP spectra revealed a monotonic increase in intensity and Nb:Si ratio with loading (Fig. S5 and Table S2), and comprised a single spin-orbit split doublet with a $3d_{5/2}$ binding energy of around 207 eV (indicative of Nb^{5+} in Nb_2O_5 [56–58]) for all loadings. The Nb:Si ratio decreased progressively with calcination temperature for Nb loadings >16 wt%, consistent with particle sintering and a concomitant lower dispersion of niobia. The Nb surface loading referred to as the surface Nb density (atoms nm^{-2}), was estimated
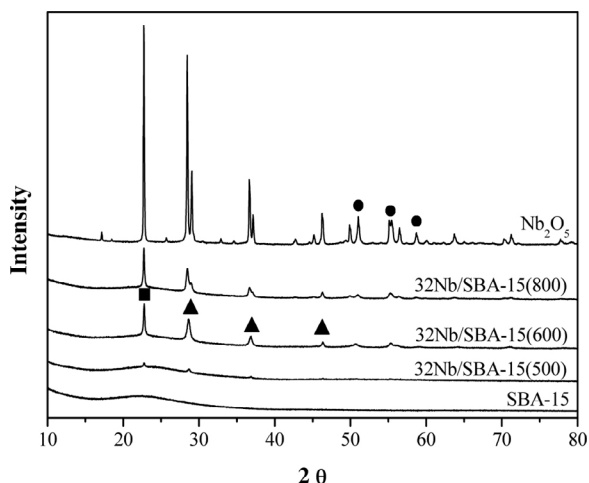

Fig. 1. XRD patterns of Nb/SBA-15 as a function of Nb loading and calcination temperature: (a) 500 °C; (b) 600 °C and (c) 800 °C. A reference pattern for commercial pure Nb_2O_5 is shown, and reflections associated with pseudohexagonal (TT, ▲), orthorhombic (T, ■) and monoclinic (α, ●) niobia indicated.
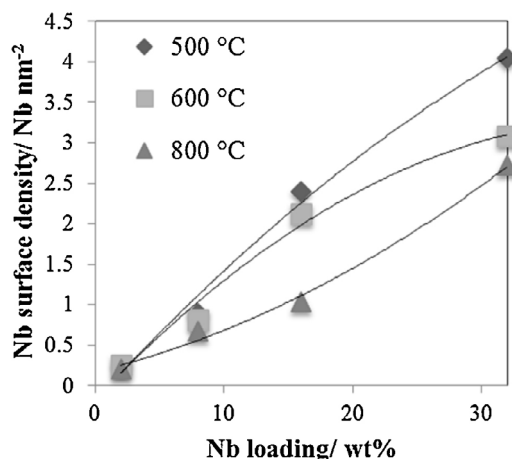
considering the weight% Nb loading (Table S2) obtained from the XPS measurements and normalizing this for the surface area (S_{BET}) (Fig. S2) using Eq. (S1) (Supplementary content) [56,58]. Fig. 3 shows how the Nb surface density (atoms nm^{-2}) for xNb/SBA-15Nb (x = 2 to 32 wt%) varies as a function of Nb loading and calcination temperature.

The linear increase in Nb surface density at 500 °C suggests that the dispersion of Nb species is greatest at this calcination temperature. The deviation from linearity at higher loading for the 600 °C calcined sample and lower surface density of Nb species for the 800 °C calcined sample suggests agglomeration occurs under these

Fig. 2. XRD patterns of 32Nb/SBA-15 as a function of calcination temperature. A reference pattern for commercial pure Nb_2O_5 is shown, and reflections associated with pseudohexagonal (TT, ▲), orthorhombic (T, ■) and monoclinic (α, ●) niobia indicated.
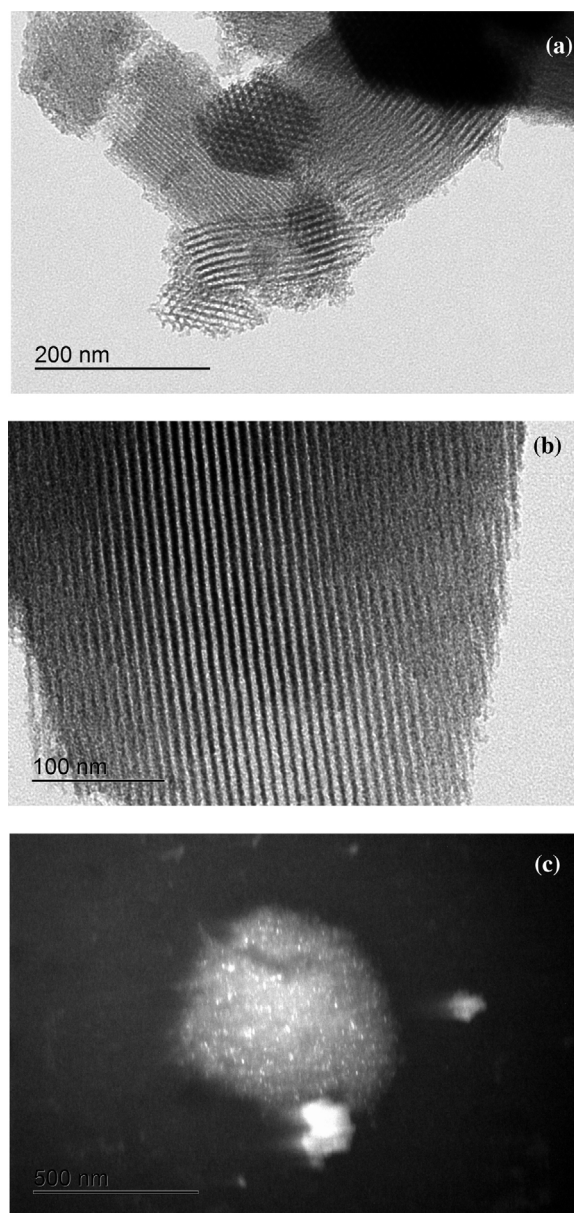

Fig. 3. Evolution of Nb surface density with Nb content as a function of calcination temperature for xNb/SBA-15 (x = 2 to 32 wt%).
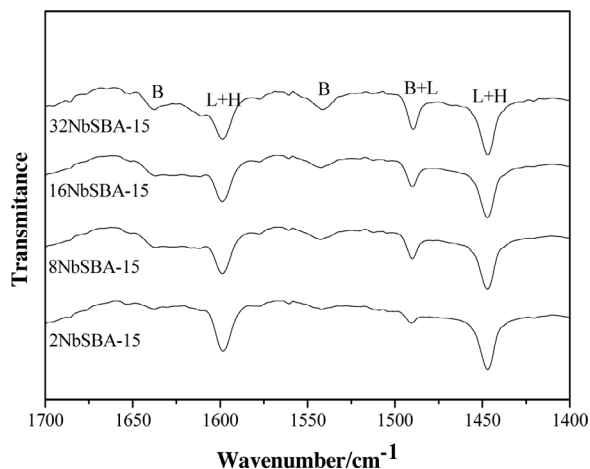

Fig. 4. Bright-field TEM images of (a) parent SBA-15, and (b) 2Nb/SBA-15(500) and (c) dark-field STEM image of 2Nb/SBA-15(500).

Fig. 5. DRIFT spectra of pyridine adsorption over xNb/SBA-15(y) (y = calcined at 500 °C) as a function of Nb loading (x = 2 to 32 wt%).
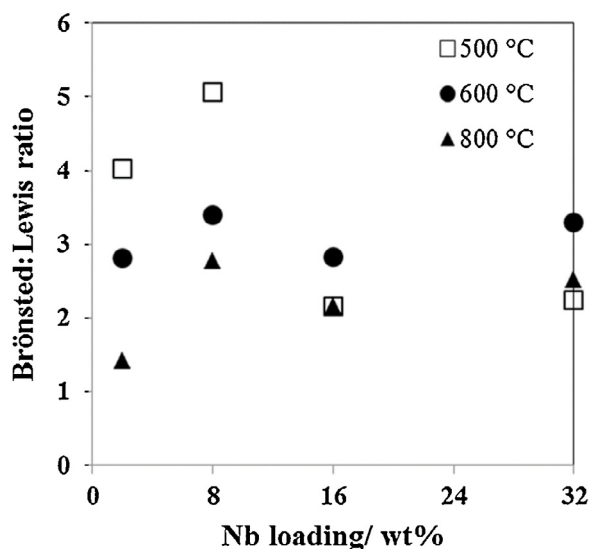
conditions lowering dispersion. Highly dispersed niobia species are expected to exist as tetrahedrally coordinated [NbO$_4$] species on silica as previously reported [59], whereas octahedrally coordinated Nb in polymeric species give rise to a band at 330 nm. Band broadening observed in our DRUV measurements for high loadings or high calcination temperatures (Fig. S4) would thus be consistent with niobium oxide cluster growth. Indeed literature suggests that tetrahedrally coordinated Nb species can form polymeric NbOx species with an octahedral structure [NbO$_6$] upon thermal processing [56]. This new Nb species can gradually dominate the surface by connection with isolated units of [NbO$_4$] and associated 3D growth.

The morphology of as-prepared 2Nb/SBA-15 was also examined by transmission electronic microscopy (TEM), with Fig. 4 highlighting the well-ordered hexagonal mesopores characteristic of the SBA-15 support and absence of any bulk-like niobia structures in agreement with XRD and DRUVS. However, dark-field STEM which is sensitive to high atomic number elements revealed a uniform distribution of small (<5 nm) niobium nanoparticles throughout the SBA-15 pore network.

DRIFTS analysis of pyridine titrated materials is a standard method for qualitative and quantitative characterization of solid acidity [60–62]. Fig. 5 shows DRIFT spectra of the 500 °C calcined xNb/SBA-15 materials as a function of Nb loading (analogous

Fig. 6. The correlation between Nb loading (x = 2 to 32 wt%) and the B/L ratio in samples xNb/SBA-15 calcined at 500, 600 and 800 °C.

spectra for 600 °C and 800 °C materials are shown in Fig. S6, Supplementary content). Bands were observed at 1450, 1578 cm^{-1} and 1610 cm^{-1}, arising from pyridine adsorption at Lewis (L) acid sites, while pyridine adsorbed at Brönsted (B) acid sites gave rise to a strong band at 1550 cm^{-1}, with an additional band at 1490 cm^{-1} associated with pyridine coordinated to both B + L sites [28,50,51]. Pyridine hydrogen weakly bonded (H) to silanols in the SBA-15 support gave only very weak bands at 1445 and 1598 cm^{-1}. The corresponding variation in Brönsted/Lewis acidity, derived from the ratio of the 1550 cm^{-1}:1610 cm^{-1} peak intensities is given in Table S3 (Supplementary content).

The results presented in Table S3 and Fig. 6 show that the B/L ratio always passes through a maximum for the 8Nb/SBA-15 sample irrespective of the calcination temperature. Calcination is expected to induce dehydroxylation of the catalyst surface which will decrease Brönsted acidity, while sintering of isolated tetrahedrally coordinated Nb species and concomitant formation of polymeric NbOx species expected to decrease the overall available acid sites [53–57]. The observed increase in Lewis acidity with loading or calcination is consistent with studies on the thermal processing of bulk Nb$_2$O$_5$·nH$_2$O [61], where calcination >300 °C led to water removal and an increase in Lewis acidity at the expense of Brönsted character. Treatment >500 °C led to a material with very weak acidity with resulting materials catalytically inactive due to the progressive recrystallization of amorphous material into the pseudohexagonal (TT) and orthorhombic (T) phase of Nb$_2$O$_5$ at 500–600 °C and 600–700 °C respectively [63], in accord with our results presented in Fig. 1 and Table S3.

3.2. Catalytic activity

The catalytic performance of xNb/SBA-15(y) materials was subsequently explored in propanoic acid esterification with methanol at 60 °C. These experimental conditions were chosen based on previous optimized studies for solid acid catalysed esterification reactions [64,65], with a high methanol content chosen to both drive the reaction equilibrium and act as a solvent to ensure good mass transport. The parent SBA-15 was inactive under these conditions, confirming the requirement for solid acidity.

Figs. 7 and S7 show the variation in propanoic acid conversion as a function of Nb loading for the 500 °C calcined series, which demonstrates the highest conversion was observed for
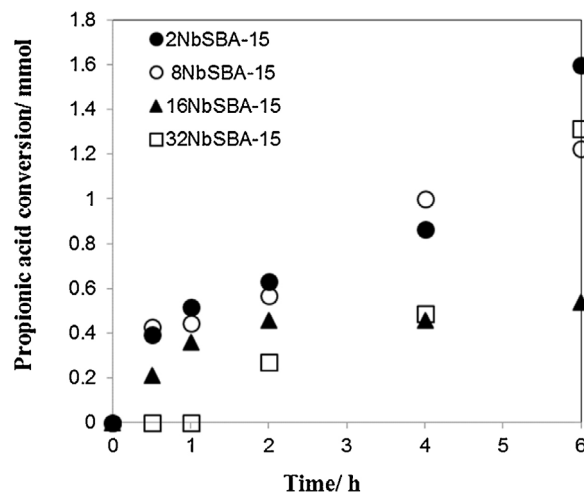

Fig. 7. Conversion profiles for the esterification of propionic acid with methanol catalyzed by xNb/SBA-15 (x = 2 to 32 wt%) calcined at 500 °C. Reactions conditions: 10 mmol of propionic acid, molar ratio MeOH/acid = 30, 50 mg of catalyst and 60 °C.

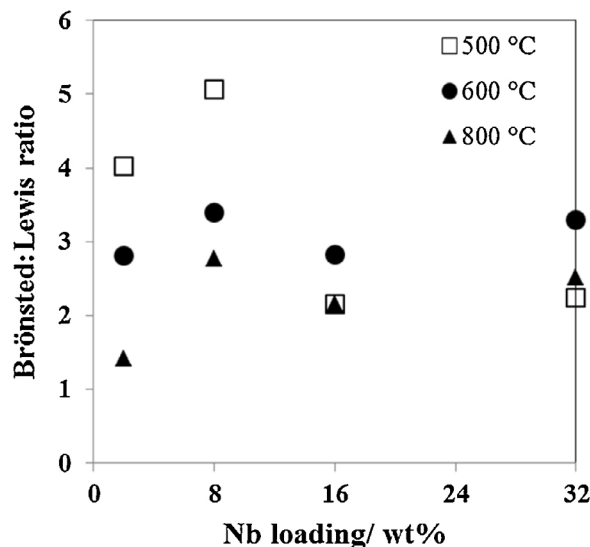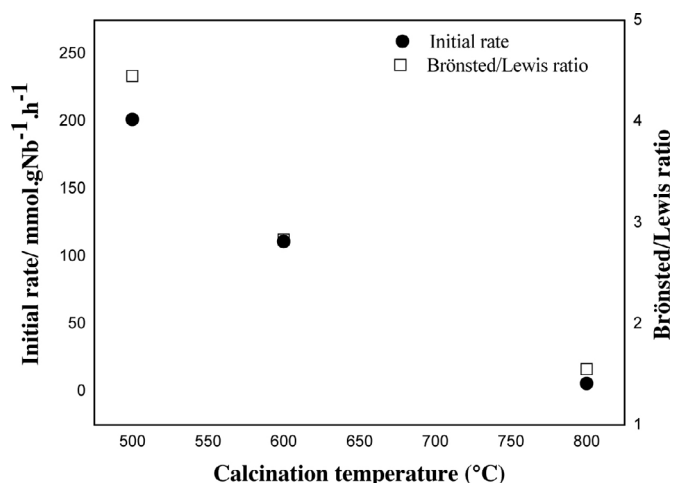**Fig. 8.** Effect of Nb loading and calcination temperature on the activity of xNb/SBA-15y in propanoic acid esterification with methanol.

2Nb and 8Nb/SBA-15, which exhibit the highest Brönsted:Lewis ratio. Propanoic acid conversion and yield of ester produced progressively decrease with Nb loading, or increased calcination temperature as shown in Fig. S7.

Fig. 8 shows a comparison of the specific activity of all the xNb/SBA-15y catalysts, calculated from normalization of the initial rates of reaction to the niobium content. In all cases this reveals the highest activity is observed for 2Nb/SBA-15y sample, with activity found to decrease with increased Nb loading. This is explicable based on the combined TEM and acidity measurements which demonstrate that 2Nb/SBA-15(500) exhibits a highly dispersed Nb species which possesses a high Brönsted:Lewis ratio. For higher Nb loadings the overall performance of the 500 and 600 °C calcined samples are very similar. However, in contrast the 800 °C calcined samples are virtually inactive which is explicable in terms of extensive recrystallisation of Nb$_2$O$_5$ into the pseudohexagonal (TT) and orthorhombic (T) phase, at this temperature as observed in the XRD (Fig. 1). Only 2Nb/SBA-15(800) shows any activity suggesting that the highly dispersed precursor is sufficiently resistant to sintering under these conditions. The detrimental effect of calcination temperature on catalytic activity is consistent with reports by

Fig. 9. Correlation between initial rate, Nb loading and B/L ratio for the solids catalysts prepared xNb/SBA-15(y) (x = 2 wt%, y = 500, 600 and 800 °C).

Ilzuka et al., who also reported thermal processing of hydrated niobia diminished the activity for 1-butene izomerization, propylene polymerization and 2-butanol dehydration due to a loss of Brönsted acidity [66]. The interdependence of catalytic activity with Nb dispersion and calcination temperature is clearly related to the ability of supported Nb species to sinter, and thus the strength of interaction with the support [67,68]. The use of strongly interacting supports that can maintain small particle sizes should be a key factor in determining the catalytic activity [69,70]. Indeed, the stability of the 2Nb/SBA-15(500) catalyst was further assessed under more aggressive solvothermal conditions, at 120 °C using a lower methanol:propanoic acid ratio of 15:1, under which conditions the acid conversions exceeded 92%, which was maintained for 4 consecutive reactions (Fig. S8), evidencing minimal deactivation.

These observations are similar to other reports where mesoporous matrices have been employed to prepare supported NbOx catalysts, and increased dispersion and stability of niobia species present at low loadings is highlighted as contributing to the increased catalytic activity and prolonged catalyst lifetime [66,69,70–72]. Garcia-Sancho et al. also reported that the Nb loading on Nb_2O_5/MCM catalysts has a significant impact on methyl ester yield in biodiesel production, with catalytic activity tracking Nb loading and acidity up to the highest loading investigated of 8 wt% Nb_2O_5 [58].

Considering in more detail the most active 2Nb/SBA-15 catalyst, a good correlation between the initial rate of esterification and evolution of acidic properties upon calcination can also be observed. Fig. 9 reveals a linear dependence of the initial rate of propanoic acid esterification on Brönsted/Lewis ratio (B/L), which clearly identifies Brönsted acidity as critical for esterification, and confirms that high temperature calcination preferentially destroys these active sites.

The formation of NbO_4 species is expected over silica supports [73], thus the formation of Si—O—Nb bonds via reaction of the $NbCl_5$ precursor with the surface hydroxyls of a high surface area mesoporous SBA-15 support should give rise to a highly dispersed form of NbO_4 as observed on MCM-41 [74]. This surface species is noted to be both chemically and thermally stable up to ~500 °C and exhibit Brönsted acidity, consistent with our observations for 2Nb/SBA- 15(500) sample. Brönsted acidity is critical for both the activation of the carboxylic and alcohol during the mechanism of fatty acid esterification [6–8,13,62]. A recent study proposes adsorption of ethanol on silica supported tetrahedral mono-oxo NbO_4 surface species gives rise to a Brönsted-acidic surface complex [75], which if also formed with methanol, could be critical for promoting esterification processes. Calcination at elevated temperatures is detrimental for Brönsted acidity and esterification activity due to progressive recrystallization of this active niobia species.

4. Conclusions

A family of SBA-15 supported niobia catalysts have prepared and characterized, with the effect of Nb loading and calcination temperature investigated for propionic acid esterification with methanol as a model reaction for biofuel production.

Characterization of the prepared catalysts demonstrated that at high niobium content and also a high calcination temperature the mesopores of SBA-15 were retained, however a moderate decrease in surface areas was observed with increasing Nb loading. XRD and DRUV measurements suggested the possibility of Nb species in extra framework positions on silica network, while XRD analysis suggested the formation of TT and T – phases of niobia can be formed and along with small amounts of the α-phase at high calcination temperature. At high loadings, the observation of a band at 330 nm by DRUV analysis suggests the presence of the octahedral Nb_2O_5 species in the analyzed solids, which was in agreement with XPS analysis. The Brönsted:Lewis ratio is found to vary as a strong function of both Nb loading and calcination temperature, with 2 and 8 wt% Nb loadings found to exhibit the highest Brönsted:Lewis ratio. The 2Nb/SBA-15(500) catalyst showed the best activity and stability even after three recycling runs. Calcination at 600 and 800 °C resulted in a decrease in Brönsted:Lewis ratio, which led to a reduction in the activity of the catalysts for esterification. This catalyst behavior strongly suggests that the niobium species responsible for the catalytic activity can be related to a highly dispersed NbO_4 species, previously reported to form on silica surfaces. Formation of such species requires reaction of the Nb precursor with surface silanol groups to form Si—O—Nb bonds, which accounts for the excellent catalyst stability.

Appendix A. Supplementary data

Supplementary data associated with this article can be found, in the online version, at http://dx.doi.org/10.1016/j.apcatb.2016.12.066.

References

[1] J. Popp, Z. Lakner, M. Harangi-Rákos, M. Fári, Renew. Sustain. Energy Rev. 32 (2014) 559.
[2] D. Pottmaier, Renew. Sustain. Energy Rev. 19 (2013) 678.
[3] M.J. Climent, A. Corma, S. Iborra, Green Chem. 16 (2014) 516.
[4] A.F. Lee, J.A. Bennett, J.C. Manayil, K. Wilson, Chem. Soc. Rev. 43 (2014) 7887.
[5] E.P.A. Rocha, F.J.B. Gomes, E. Sermyagina, M. Cardoso, J.L. Colodette, Energy Fuel 29 (2015) 7975.
[6] G. Knothe, Green Chem. 13 (2011) 3048.
[7] F. Ma, A. Hanna, Bioresour. Technol. 70 (1999) 1.
[8] U. Schuchardt, R. Serchelia, R.M. Vargas, J. Braz, Chem. Soc. 9 (1998) 199.
[9] O.E. Ajala, F. Aberuagba, T.E. Odetoye, A.M. Ajala, Chem. Biol. Eng. Rev. 2 (3) (2015) 145.
[10] K. Kohse-Hinghaus, P. Oßwald, T.A. Cool, T. Kasper, N. Hansen, F. Qi, C.K. Westbrook, P.R. Westmoreland, Angew. Chem. 49 (2010) 3572.
[11] R. Luque, J.C. Lovett, B. Datta, J. Clancy, J.M. Campelo, A.A. Romero, Energy Environ. Sci. 3 (2010) 1706.
[12] I.A.L. Bassan, D.R. Nascimento, R.A.S. Gil, M.I.P. da Silva, C.R. Moreira, W.A. Gonzalez, A.C. Faro Jr., T. Onfroy, E.R. Lachter, Fuel Process. Technol. 106 (2013) 619.

[13] E. Lotero, Y. Liu, D.E. Lopes, K. Suwannakarn, D.A. Bruce, J.G. Goodwin, Ind. Eng. Chem. Res. 44 (14) (2005) 5353.
[14] K. Narasimharao, D.R. Brown, A.F. Lee, A.D. Newman, P.F. Siril, S.J. Tavener, K. Wilson, J. Catal. 248 (2007) 226.
[15] L. Pesaresi, D.R. Brown, A.F. Lee, J.M. Montero, H. Williams, K. Wilson, Appl. Catal. A: Gen. 360 (2009) 50.
[16] J. Dhainaut, J.-P. Dacquin, A.F. Lee, K. Wilson, Green Chem. 12 (2010) 296.
[17] C. Pirez, A.F. Lee, J.C. Manayil, C.M.A. Parlettb, K. Wilson, Green Chem. 16 (2014) 4506.
[18] X. Mo, E. Lotero, C. Lu, Y. Liu, J.G. Goodwin, Catal. Lett. 123 (2008) 1.
[19] R. Purova, K. Narasimharaoa, N.S.I. Ahmeda, S. Al-Thabaiti, A. Al-Shehri, M. Mokhtar, W. Schwieger, J. Mol. Catal. A: Chem. 406 (2015) 159.
[20] D.A.G. Aranda, J.A. Gonçalves, J.S. Peres, A.L.D. Ramos, C.A.R. de Melo Jr., O.A.C. Antunes, N.C. Furtado, C.A. Taft, J. Phys. Org. Chem. 22 (2009) 709.
[21] I.A.L. Bassan, D.R. Nascimento, Fuel Process. Technol. 106 (2013) 619.
[22] A. Corma, Chem. Rev. 97 (1997) 2373.
[23] G. Morales, A. Osatiashtiani, B. Hernandez, J. Iglesias, J.A. Melero, M. Paniagua, D.R. Brown, M. Granollers, A.F. Lee, K. Wilson, Chem. Commun. 50 (2014) 11742.
[24] A. Osatiashtiani, A.F. Lee, M. Granollers, D.R. Brown, L. Olivi, G. Morales, J.A. Melero, K. Wilson, ACS Catal. 5 (2015) 4345.
[25] J.J. Creasey, C.M.A. Parlett, J.C. Manayil, M.A. Isaacs, K. Wilson, A.F. Lee, Green Chem. 17 (2015) 2398.
[26] V. Calvino-Casilda, M. Olejniczak, R.M. Martín-Aranda, M. Ziolek, Microporous Mesoporous Mater. 224 (2016) 201.
[27] M. Olejniczak, M. Ziolek, Microporous Mesoporous Mater. 196 (2014) 243.
[28] M. Trejda, K. Stawicka, A. Dubinska, M. Ziolek, Catal. Today 187 (2012) 129.
[29] I. Nowak, Catal. Today 192 (2012) 80.
[30] S. Sumiya, Y. Oumi, M. Sadakane, T. Sano, Appl. Catal. A: Gen. 365 (2009) 261.
[31] D. Zhao, J. Feng, Q. Huo, N. Melosh, G.H. Fredrickson, B.F. Chmelka, G.D. Stucky, Science 279 (1998) 548.
[32] Y. Wan, D. Zhao, Chem. Rev. 107 (2007) 2822.
[33] H.-J. Chae, T.-W. Kim, Y.-K. Moon, H.-K. Kim, K.-E. Jeong, C.-U. Kim, S.-Y. Jeong, Appl. Catal. B: Environ. 150–151 (2014) 596.
[34] M.S.P. Francisco, Y. Gushikem, J. Mater. Chem. 12 (2002) 2552.
[35] I. Nowak, M. Ziolek, Chem. Rev. 99 (1999) 3603.
[36] T. Okuhara, Chem. Rev. 102 (2002) 3641.
[37] C. Nico, T. Monteiro, M.P.F. Graça, Prog. Mater. Sci. 80 (2016) 1.
[38] C. Valencia-Balvín, S. Pérez-Walton, G.M. Dalpian, J.M. Osorio-Guillén, Comp. Mater. Sci. 81 (2014) 133.
[39] M. Ristić, S. Popović, S. Musić, Mater. Lett. 58 (2004) 2658.
[40] A. Arone, E. Marenna, V. Califano, E. Fanelli, P. Pernice, M. Trifuoggi, A. Vergara, Sol Gel Sci. Technol. 43 (2007) 193.
[41] M.P.F. Graça, A. Meireles, C. Nico, M.A. Valente, J. Alloy Compd. 553 (2013) 177.
[42] V.V. Atuchin, I.E. Kalabin, V.G. Kesler, N.V. Pervukhina, J. Electron. Spectrosc. 142 (2005) 129.
[43] A. Dacca, G. Gemme, L. Mattera, R. Parodi, Appl. Surf. Sci. 126 (1998) 219.
[44] S. Denofre, Y. Gushikem, S.C. Castro, Y. Kawano, J. Chem. Soc. Faraday Trans. 89 (1993) 1057.
[45] S. Morselli, P. Moggi, D. Cauzzi, G. Predieri, Stud. Surf. Sci. Catal. 118 (1998) 763.
[46] J.N. Kondo, K. Domen, Chem. Mater. 20 (2008) 835.
[47] D.C. Tranca, A. Wojtaszek-Gurdak, M. Ziolek, F. Tielens, Phys. Chem. Chem. Phys. 17 (2015) 22402.
[48] V. Pârvulescu, V.I. Pârvulescu, P. Grange, Catal. Today 57 (2000) 193.
[49] S.S. Rossatto, P.T. Sotomayor, L.T. Kubota, Y. Gushikem, Electrochim. Acta 47 (2002) 4451.
[50] I. Nowak, Stud. Surf. Sci. Catal. 154 (2004) 2936.
[51] M. Trejda, K. Stawicka, M. Ziolek, Appl. Catal. B: Environ. 103 (2011) 404.
[52] M. Trejda, A. Tuel, J. Kujawa, B. Kilos, M. Ziolek, Microporous Mesoporous Mater. 110 (2008) 271.
[53] J.M.R. Gallo, I.S. Paulino, U. Schuchardt, Appl. Catal. A: Gen. 266 (2004) 223.
[54] B. Kilos, A. Tuel, M. Ziolek, J.C. Volta, Catal. Today 118 (2006) 416.
[55] B. Kilos, I. Nowak, A. Tuel, M. Ziolek, J.C. Volta, Stud. Surf. Sci. Catal. 158 (2005) 1461.
[56] Z. Ma, X. Wu, Z. Si, D. Weng, J. Ma, T. Xu, Appl. Catal. B: Environ. 179 (2015) 380.
[57] V.V. Atuchin, I.E. Kalabrin, V.G. Kesler, N.V. Pervukhina, J. Electron. Spectrosc. Relat. Phenom. 142 (2005) 129.
[58] C. García-Sancho, R. Moreno-Tost, J.M. Mérida-Robles, J. Santamaría-González, A. Jiménez-López, P. Maireles-Torres, App. Catal. B: Environ. 108–109 (2011) 161.
[59] X. Gao, I.E. Wachs, M.S. Wong, J.Y. Ying, J. Catal. 203 (2001) 18.
[60] G. Busca, Catal. Today 41 (1998) 191.
[61] S. Khabtou, T. Chevreau, J.C. Lavalley, Microporous Mater. 3 (1994) 133.
[62] M.L. Marin, G.L. Hallett-Tapley, S. Impellizzeri, C. Fasciani, S. Simoncelli, J.C. Netto-Ferreira, J.C. Scaiano, Catal. Sci. Technol. 4 (2014) 3044.
[63] E.I. Ko, J.G. Weissman Catal, Today 8 (1990) 27.
[64] A.C.C. Bacilla, M.R. Freitas, A. Bail, V.C. dos Santos, N. Nagata, A. Silva, L. Marçal, K.J. Ciuffi, S. Nakagaki, J. Mol. Catal. A: Chem. 422 (2016) 221.
[65] A. Bail, V.C. dos Santos, M.R. deFreitas, L.P. Ramos, W.H. Schreiner, G.P. Ricci, K.J. Ciuffi, S. Nakagaki, Appl. Catal. B: Environ. 130–131 (2013) 314.
[66] T. Ilzuka, K. Ogasawara, K. Tanabe, Bull. Chem. Soc. Jpn. 56 (1983) 2927.
[67] I. Nowak, M. Ziolek, Chem. Rev. 99 (1999) 3603.
[68] G. Deo, I.E.J. Wachs, J. Catal. 129 (1991) 307.
[69] M. Haruta, Catal. Today 36 (1997) 153.
[70] W.-H. Wang, G.-Y. Cao, Chin. J. Chem. 24 (2006) 817.
[71] K. Tanabe, Catal. Today 8 (1990) 1.
[72] K. Tanabe, Catal. Today 78 (2003) 65.
[73] J.M. Jehng, I.E. Wachs, J. Phys. Chem. 95 (1991) 7373.
[74] X. Gao, I.E. Wachs, M.S. Wong, J.Y. Ying, J. Catal. 203 (2001) 18.
[75] M.M. Maronna, E.C. Kruissink, R.F. Parton, F. Soulimani, B.M. Weckhuysen, W.F. Hoelderich, Phys. Chem. Chem. Phys. 18 (2016) 22636.